JOURNAL OF Materials CHEMISTRY

Determination of the fluorite related structure of $Mn_3Ta_2O_8$, using synchrotron X-ray powder and electron diffraction data

Saeid Esmaeilzadeh,[a] Jekabs Grins[a] and Andy Fitch[b]

[a] *Department of Inorganic Chemistry, Arrhenius Laboratory, Stockholm University, SE-106 91 Stockholm, Sweden*
[b] *ESRF, BP 220, F-380 43 Grenoble Cedex, France*

Received 29th June 1998, Accepted 4th August 1998

The Mn^{2+}-containing oxide $Mn_3Ta_2O_8$ has been synthesised at 1200 °C in Ar atmosphere, and its structure has been solved from X-ray synchrotron powder data ($\lambda \approx 0.65$ Å) by direct methods. The structure was refined by the Rietveld method to $R_F = 6.3\%$, with space group $I4_1/a$, $a = 11.2728(2)$, $c = 9.8030(3)$ Å, $V = 1243.47$ Å^3, from 1190 reflections with $d \geqslant 0.65$ Å. It is related to the fluorite structure with $a \approx \sqrt{5}a_f$ and $c \approx 2a_f$. The Ta atoms are octahedrally coordinated by oxygen atoms and the three crystallographically different Mn atoms by 7, 4 + 4 and 4 oxygen atoms. Electron diffraction patterns show the presence of weak superstructure reflections corresponding to a primitive unit cell with $a' = a$ and $c' = 6c$. The melting point of $Mn_3Ta_2O_8$ is 1470 °C in Ar atmosphere. It is a semiconductor with an activation energy of 1.2 eV and a conductivity $\sigma = 3.7 \times 10^{-5}$ S cm^{-1} at 600 °C. The magnetic susceptibility shows a maximum at 23 K and a Curie–Weiss behaviour at higher temperatures, with $\mu_{eff} = 5.7(1)\ \mu_B$ per Mn atom. When $Mn_3Ta_2O_8$ is oxidised at 1100 °C in air an Mn–Ta oxide forms, which has a wolframite type structure with unit cell $a = 4.7574(5)$, $b = 5.7296(6)$, $c = 5.1133(4)$ Å and $\beta = 91.202(9)°$.

Introduction

The phase relations of Mn-Ta oxides have been investigated by Turnock,[1] at 1200 °C and partial pressures of oxygen from 10^{-17} to 1 atm. The oxides observed were the orthorhombic columbite-type $MnTa_2O_6$, $Mn_4Ta_2O_9$ with a corundum-related structure, and four compounds, $MnTaO_4$, $Mn_{1.4}TaO_{4.2}$, $Mn_{1.4}TaO_{3.9}$ and $Mn_6Ta_2O_{11}$, with structures undetermined at the time. Two additional Mn–Ta oxides have been reported by Schönberg,[2] namely the metallic compound Mn_3Ta_3O with the η-carbide type structure and Mn_2TaO_3 with an alleged CoSn (B35 type) structure. The latter of these phases appears to be quite unique and questionable, considering the low oxidation state of Ta.

Several of the above Mn^{2+}-containing Mn–Ta oxides were prepared by us for use as precursor materials in the synthesis of new Mn–Ta oxynitrides.[3] Since the structures of most of them, including '$Mn_6Ta_2O_{11}$' and '$Mn_{1.4}TaO_{3.9}$', were not known, we have investigated their structures and properties. A study of '$Mn_6Ta_2O_{11}$' showed that the correct composition is $Mn_{11}Ta_4O_{21}$.[4] The crystal structure is trigonal (space group) with $a = 5.3776(2)$, $c = 34.040(2)$ Å and can be described as built up from corundum-type $Mn_4Ta_2O_9$ blocks alternating with single MnO layers of octahedra.

The compound $Mn_3Ta_2O_8$ is the oxide described by Turnock as '$Mn_{1.4}TaO_{3.9}$'. The present study comprises a determination of its structure and characterisation of its thermal, magnetic and electrical properties. The structure is found to be related to the cubic MX_2 fluorite type. A vast variety of structure types can be derived from fluorite by ordered removal of the X atoms and/or ordering of metal atoms, among them the $A_2B_2X_7$ ($MX_{1.75}$) pyrochlore[5] and the rare-earth RE_2X_3 ($MX_{1.5}$) *C*-type.[6] $Mn_3Ta_2O_8$ ($MX_{1.6}$) is a new type within the class of MX_2 fluorites and related structures.

Experimental

Samples of $Mn_3Ta_2O_8$ were prepared by solid state reaction in Ar atmosphere, using a mixture of appropriate amounts (3:1) of $Mn(C_2O_4)$ and fine-grained Ta_2O_5, heated in Ni crucibles in a graphite furnace. The samples were fired at 900 °C for 12 h and then at 1200 °C for 12 h, with intermediate grinding and re-pelleting. The obtained sintered pellets were brown. Higher and lower Mn contents yielded materials with $Mn_4Ta_2O_9$ and $MnTa_2O_6$, respectively, as secondary phases. Corresponding syntheses above 1350 °C yielded partially melted materials that contained $Mn_4Ta_2O_9$ as the major phase. The $Mn_3Ta_2O_8$ phase was described by Turnock[1] as $Mn_{1.4}TaO_{3.9}$, stable only above 1160 °C and oxygen partial pressures below *ca.* 2.5×10^{-2} atm. at 1200 °C.

A Guinier–Hägg camera with Cu-Kα_1 radiation was used for collection of powder diffraction patterns for phase identification. The films were measured with a computer-controlled microdensitometer.

X-Ray powder diffraction data for structure determination and refinement were collected from a sample contained in a 0.2 mm diameter spinning capillary on beam line BM16 at the ESRF, Grenoble, with $\lambda = 0.652\,782(3)$ Å, in the 2θ range 1–57°. The detector arm, with its nine detectors, was scanned at a continuous rate of 0.5 degrees min^{-1}, and the electronic scalers and 2θ encoder were read every 200 ms. The data were subsequently normalised and rebinned, and the counts from the nine channels combined, to yield the equivalent scan with a step of 0.002°. The direct methods program SIRPOW91[7] was used for solving the structure and the GSAS program package[8] for structure refinements.

Metal elemental analyses were made in a JEOL 820 SEM (scanning electron microscope) with the EDX (energy dispersive X-ray) analysis system LINK 10000.

A JEOL 2000 FX microscope, operated at 200 kV, and with a double tilting goniometer with limitations of ±45°, was used for collecting electron diffraction (ED) patterns. The specimens were crushed, dispersed in butanol, and then transferred to holey carbon-coated copper grids.

Thermal analysis was carried out with a SETARAM Labsys TG-DTA16 instrument. The recordings were made in both Ar atmosphere and air, and with heating/cooling rates of 5–10 °C min^{-1}.

The magnetic susceptibility was measured with a weak-field ac-susceptometer (Lake Shore 7130) in the temperature range 10–300 K, using a magnetic field of 500 A m^{-1} and a frequency of 500 Hz.

The electrical conductivity was determined with an automated impedance spectrometer.[9] Data were collected at 400–600 °C in the frequency range 10 Hz–1 MHz. The measurements were made in N_2 atmosphere on sintered discs, 0.5 cm^2 in area and 0.1 cm thick, with a porosity of *ca.* 20%, and furnished with gold electrodes.

Results

Compositional analysis

SEM investigations of polished surfaces of sintered $Mn_3Ta_2O_8$ compacts revealed an average crystallite size of 10 μm. Twenty EDX point analyses on individual grains yielded a metal composition of 61(1) % Mn and 39(1)% Ta, in agreement with the starting composition.

X-Ray powder diffraction

The Guinier–Hägg powder pattern of $Mn_3Ta_2O_8$ was indexed with a body-centred unit cell, using the TREOR90 version of the indexing program TREOR.[10] The cell dimensions $a=11.2728(2)$, $c=9.8030(3)$ Å were obtained, using Si as internal standard and 80 reflections for $2\theta<88°$. The indexed powder pattern is given in Table 1 for the first 20 observed lines. It agrees with that given by Turnock[1] but contains additional weak reflections and the recorded *d* values are more accurately determined. Systematic absences in the powder pattern ($hk0$, $h,k\neq 2n$;$00l$, $l\neq 4n$) indicated the space group $I4_1/a$ to be possible. The pattern showed furthermore that the sample contained small amounts of $Mn_4Ta_2O_9$ and $MnTa_2O_6$ as impurities.

Structure determination and refinement

The synchrotron powder pattern did not exhibit any more Bragg reflections than those observed in Guinier–Hägg films, and could thus not validate the lower symmetry and larger unit cell implied by the ED study (see below). It was therefore decided to solve the structure using the unit cell obtained from the X-ray data, with $a\approx 11.3$ and $c\approx 9.8$ Å.

Observed integrated intensities were extracted from a part of the synchrotron data and converted to $|F|^2$ values. A partial structure was then derived in space group $I4_1/a$ by direct methods. The SIRPOW91 program successfully located the positions of the metal atoms and three out of the four oxygen atoms. The remaining fourth oxygen atom was later located from difference Fourier maps.

Table 1 Observed and calculated 2θ values for the Guinier–Hägg diffraction pattern of $Mn_3Ta_2O_8$ up to the twentieth observed line. $\Delta 2\theta=2\theta_{obs}-2\theta_{calc}$. [$\lambda=1.5406$ Å, cell figure-of-merit: $M_{20}=98$, $F_{20}=133$ (0.0060, 26)].

hkl	$2\theta_{obs}$/degrees	$\Delta 2\theta$	d_{obs}/Å	I/I_0
1 0 1	11.955	0.001	7.40	7
2 0 0	15.704	−0.006	5.64	1
1 2 1	19.785	−0.002	4.484	43
1 1 2	21.256	−0.007	4.177	8
2 2 0	22.292	0.005	3.985	7
3 0 1	25.363	−0.001	3.509	14
1 0 3	28.424	0.009	3.137	6
2 3 1	29.964	−0.011	2.980	2
3 1 2	30.977	−0.017	2.885	100
2 1 3	32.629	−0.002	2.742	11
4 1 1	34.017	0.003	2.633	3
4 2 0	35.576	−0.011	2.521	24
3 0 3	36.418	0.010	2.4651	1
0 0 4	36.636	−0.002	2.4509	9
3 3 2	38.501	−0.009	2.3364	1
3 2 3	39.881	0.007	2.2587	3
4 2 2	40.203	0.006	2.2413	2
5 0 1/4 3 1	41.044	−0.002	2.1973	11
4 1 3	43.112	0.007	2.0966	3
2 2 4	43.308	0.002	2.0875	1

Table 2 Atomic coordinates for $Mn_3Ta_2O_8$; [tetragonal, $a=11.2782(2)$ Å, $c=9.8030(3)$ Å, $I4_1/a$, $Z=4$].

Atom	Site	*x*	*y*	*z*	U/Å^2
Ta	16f	0.42257(7)	0.05661(9)	0.1300(1)	0.00641(2)
Mn1	16f	0.3780(5)	0.0505(3)	0.5949(3)	0.0077(1)
Mn2	4a	0	1/4	1/8	0.0073(2)
Mn3	4b	0	1/4	5/8	0.0071(2)
O1	16f	0.362(1)	0.198(1)	0.221(1)	0.0043(3)
O2	16f	0.460(1)	0.893(1)	0.013(1)	0.0043(2)
O3	16f	0.196(1)	0.312(1)	0.997(1)	0.0056(3)
O4	16f	0.310(1)	0.961(1)	0.243(1)	0.0048(2)

The structure was refined using 1190 reflections in the 2θ range 5–57° ($d\geqslant 0.65$ Å). The background was fitted by 20 Chebyshev polynomial coefficients. The half-width of the Bragg peaks was 0.014° at $2\theta=21.4°$. $MnTa_2O_6$ and $Mn_4Ta_2O_9$ were included as secondary phases, with collective thermal parameters, lattice parameters and phase fractions refined. A total of 74 parameters were refined, including 18 positional and 8 thermal parameters for $Mn_3Ta_2O_8$. The obtained atomic coordinates are given in Table 2. Selected interatomic distances and bond valence sums[11] are given in Table 3, together with expected bond distances, calculated from Shannon–Prewitt ionic radii:[12] O^{2-}(IV) = 1.38 Å, Ta^{5+}(VI) = 0.64 Å, Mn^{2+}(HS,IV) = 0.66 Å, Mn^{2+}(HS,VII) = 0.90 Å, Mn^{2+}(HS,VIII) = 0.96 Å. The fit between observed and calculated patterns is illustrated in Fig. 1. The corresponding refinement indices are $R_{wp}=0.100$, $R_p=0.071$, $DwD=0.90$, $R_F=0.063$ and $\chi^2=4.8$. The refined phase fractions of $MnTa_2O_6$ and $Mn_4Ta_2O_9$ were 8.7(1) and 1.5(1) wt.%, respectively, corresponding to a total Mn content of 58.3%.

Table 3 Bond distances (Å) and bond valence sums for $Mn_3Ta_2O_8$.

Ta–O3	1.94(2)	Mn1–O3	1.98(2)	Mn2–O4	4 × 2.24(1)
O1	1.95(1)	O3	2.06(1)	O4	4 × 2.63(1)
O4	2.00(1)	O1	2.18(1)	mean 2.44, expected 2.34	
O2	2.01(1)	O1	2.34(1)		
O4	2.02(1)	O2	2.44(1)	Mn3–O2	4 × 2.00(1)
O2	2.21(1)	O4	2.47(1)	mean 2.00, expected 2.04	
		O4	2.57(1)		
mean 2.02, expected 2.02		mean 2.29, expected 2.28			

bond valence sums:				
Ta	+4.74	O1	−1.86
Mn1	+2.07	O2	−1.93
Mn2	+1.51	O3	−2.12
Mn2	+2.29	O4	−1.86

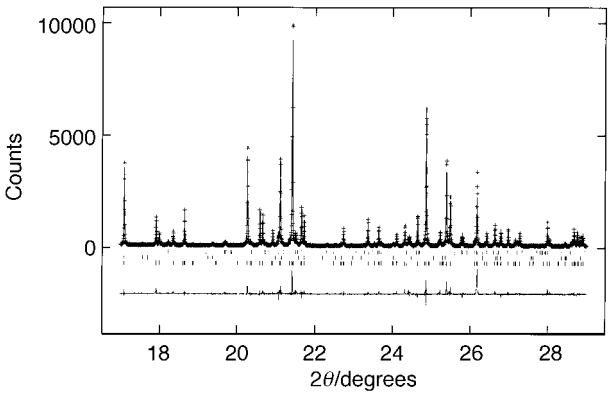

Fig. 1 Observed (crosses), calculated (solid line) and difference (bottom) X-ray diffraction patterns of $Mn_3Ta_2O_8$ for $2\theta=17$–29°.

Electron diffraction

ED patterns of $Mn_3Ta_2O_8$ showed reflections that matched the I-centred unit cell, with $a \approx 11.3$ and $c \approx 9.8$ Å, that was derived from the X-ray data, but also sets of weaker reflections that implied both a lower symmetry and a larger unit cell. These superstructure reflections were yielded by all crystallites studied.

Diffraction patterns along [001], [10$\bar{3}$] and [$\bar{1}$02] are shown in Fig. 2. The strongest reflections in the $<001>$ zone [Fig. 1(a)] correspond to a fluorite-type subcell. The a axis of the I-centred unit cell is defined by the reciprocal lattice vector $a^* = 1/5(2a^*_f + b^*_f)$, as illustrated. The presence of weaker reflections of the type 100 shows, however, that the cell is primitive, and thus also that the glide plane perpendicular to the a axis is absent. This suggests $P4_1$ or $P\bar{4}$ as possible space group symmetries. The radius of the first order Laue zone indicated furthermore a c axis of *ca.* 30 Å. The crystal was then tilted around the b axis. In the [10$\bar{3}$] zone [Fig. 1(b)] there are relatively strong superstructure reflections with indices such as 1 0 1/3 and 2 0 2/3, which can be accounted for by a primitive cell with a tripled c axis. In the [$\bar{1}$02] zone [Fig. 1(c)] there are weak reflections present with indices such as 1 0 1/2, implying a doubled c axis. The smallest unit cell able to index all reflections is thus found to be a primitive tetragonal with $a' = a$ and $c' = 6c \approx 58.8$ Å. The sets of superstructure reflections have different relative intensities. Those that indicate a tripled c axis are the strongest, the ones that indicate a primitive cell are moderately strong, and the ones indicating a doubled c axis are the weakest.

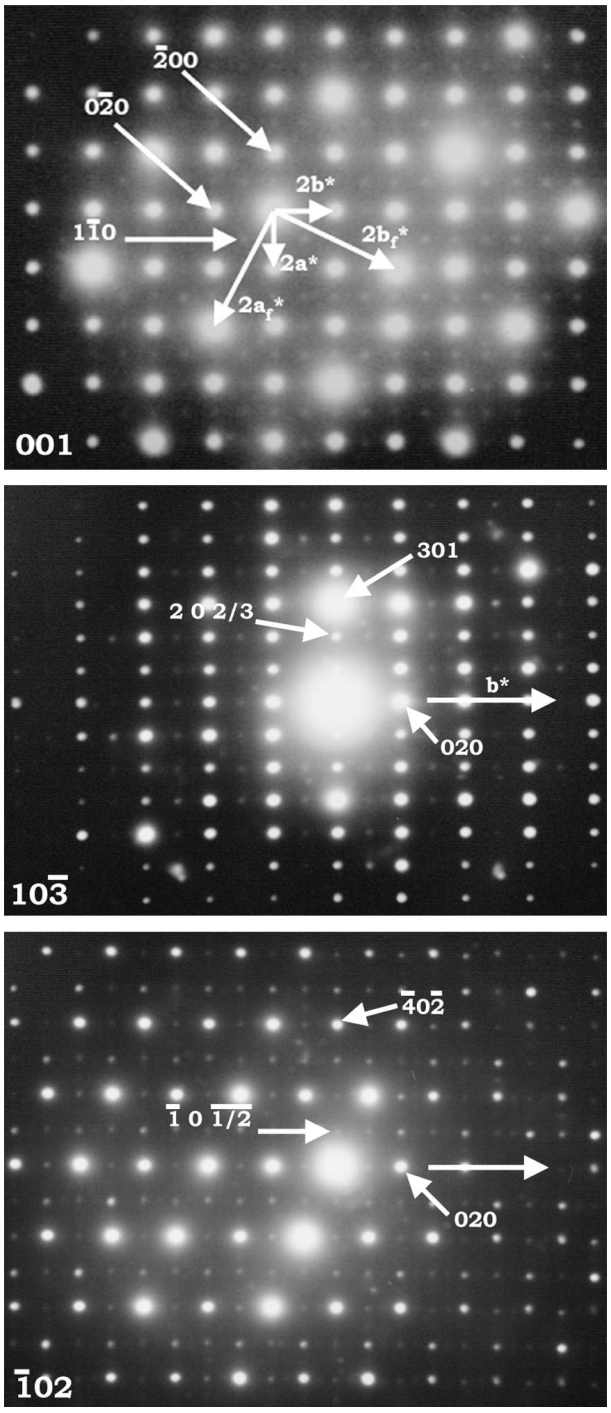

Fig. 2 Electron diffraction patterns for $Mn_3Ta_2O_8$ along (a) [001], (b) [10$\bar{3}$] and (c) [$\bar{1}$02].

Attempts were made to refine the structure both with a lower symmetry and/or larger unit cells, as implied by the electron diffraction data. Space group symmetries such as $I\bar{4}$, $P\bar{4}$ and $P4_1$ and larger unit cells with $c' = 3c$ and $c' = 6c$ were tried. None of these refinements yielded any significant improvements. This was partly expected, since the powder pattern manifests no reflections corresponding to a primitive or larger cell and any information about a superstructure is thus provided only by the main reflections. Refinements with anisotropic thermal parameters were also carried out, in order to see if any atoms would show anomalous thermal displacements, but none were revealed, and these refinements yielded only insignificantly lower R values.

Structure description

The structure derived for $Mn_3Ta_2O_8$ is illustrated in Fig. 3. There are four different metal positions, one occupied by Ta and three by Mn atoms. The metal atoms are nearly in cubic close packing, and the positional shifts from the metal array found in a cubic fluorite structure are small. The metal cubo-octahedra around the Mn and Ta atoms are only slightly distorted and the metal–metal distances have a mean value of 3.54 Å and range between 3.23 and 3.81 Å.

The structure can be envisaged as built up from four layers of metal–oxygen atom polyhedra that are related to each other by the 4_1 axis in the c direction. One such layer is shown in Fig. 3(a). The Ta atoms are coordinated by six O atoms forming a distorted octahedron, a common coordination polyhedron for Ta^{5+}. The Ta–O mean distance is 2.023 Å, which agrees well with an expected value of 2.02 Å. The structure contains pairs of Ta–O octahedra that share an edge, and these pairs are in turn connected to each other by corner-sharing. The framework formed by the Ta–O octahedra is illustrated in Fig. 3(b).

The Mn1 atoms are coordinated by seven O atoms at distances of 1.98(2)–2.57(1) Å. The coordination polyhedra can be idealised as a cube with one corner missing. The mean distance, 2.29 Å, agrees well with an ionic radius sum of 2.28 Å for Mn^{2+}(HS,VII) and O^{2-}(IV). The Mn1 atoms are located at positions that are displaced from the Ta atom positions by $z \approx 1/2$. The structure thus contains strings of Mn1–empty–Ta–empty polyhedra along the c axis, related to each other by a $\bar{4}$ symmetry axis.

The Mn2 and Mn3 atoms are found on the special positions 4a and 4b, respectively, both with site symmetries $\bar{4}$, in the channels between the Mn1–Ta strings of polyhedra, as seen in Fig. 3(b). The Mn2 atoms are 4+4 coordinated by O4 atoms at distances of 2.24(1) and 2.63(1) Å. Each set of O4 atoms forms a tetrahedron and the resulting 8-coordination polyhedron may be described as a distorted cube. The mean Mn2–O distance is 2.44 Å, which is longer than the expected value of 2.34 Å. Mn3 is tetrahedrally coordinated by four O2 atoms. The observed Mn3–O2 distance, 2.00(1) Å, is somewhat shorter than the expected value of 2.04 Å. Bond valence sums accord with the above bond-length considerations. While

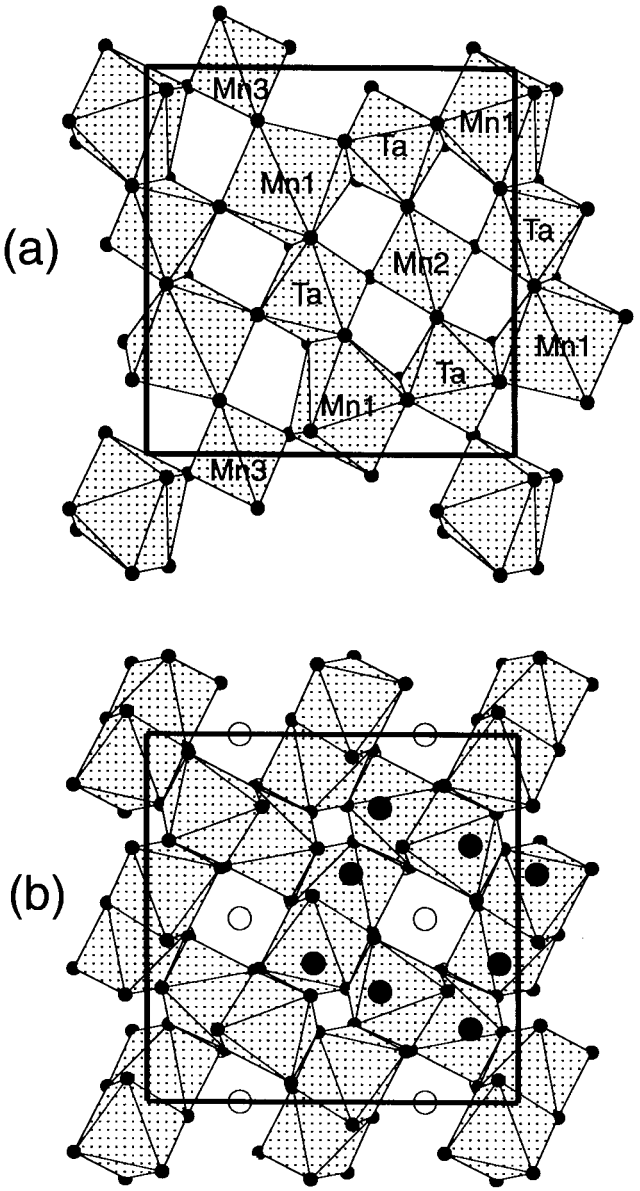

Fig. 3 An illustration of the structure of $Mn_3Ta_2O_8$: (a) a polyhedral representation of a (001) section of the structure; (b) a polyhedral representation of the Ta atom arrangement. The positions of the Mn1 and Mn2/Mn3 atoms are illustrated by filled and open circles, respectively.

they are reasonably satisfactory for the Ta, Mn1 and O atoms, too high and too low values are obtained for Mn3 and Mn2, respectively.

Magnetic susceptibility

The magnetic susceptibility per Mn atom, χ_M, of $Mn_3Ta_2O_8$ and its inverse, $\chi_M{}^{-1}$, are shown in Fig. 4 as functions of the temperature, T. The susceptibility shows a well-defined maximum at 23 K and a Curie–Weiss law behaviour $\chi_M = C/(T-\theta)$ above *ca.* 100 K. The effective number of Bohr magnetons per Mn atom (μ_{eff}) was determined from the Curie constant C to be 5.7(1) μ_B, which is close to the expected value of 5.9 μ_B for Mn^{2+} in a high-spin state.

Electrical conductivity

Impedance spectra for $Mn_3Ta_2O_8$ were measured in a heating–cooling cycle between 400 and 600 °C. The data showed no polarisation at the electrodes, and the conductivities were calculated from the low-frequency parts of the spectra. The

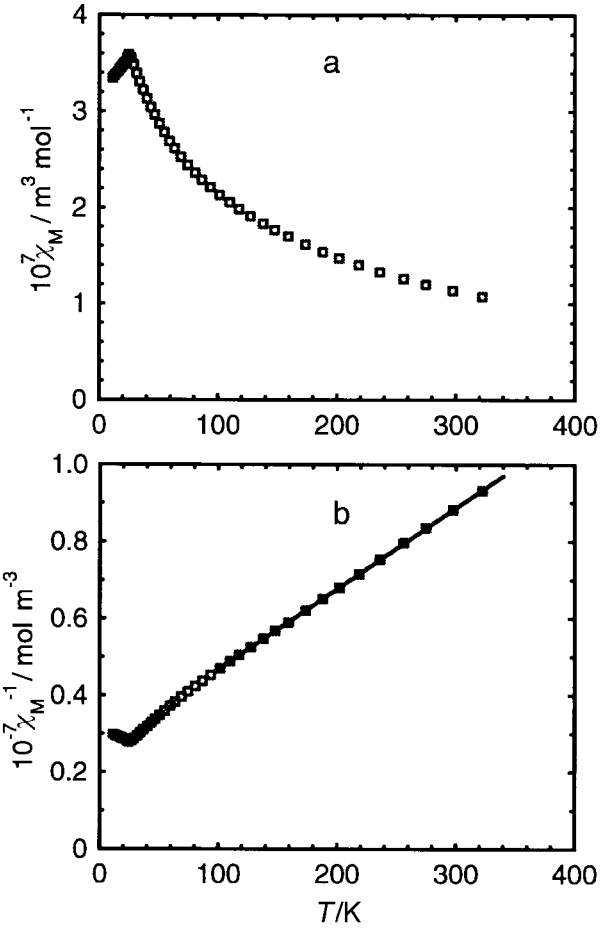

Fig. 4 Molar magnetic susceptibility per Mn atom (a) and its inverse (b) *versus* temperature for $Mn_3Ta_2O_8$.

conductivity determined at 600 °C was $\sigma = 3.7 \times 10^{-5}$ S cm^{-1} and the relative dielectric constant was calculated from the capacitance to be 30. The temperature dependence of the conductivity was found to be characteristic of a semiconductor, with an approximate activation energy value of 1.2 eV.

Thermal analysis

A DTA recording for $Mn_3Ta_2O_8$ heated and then cooled in inert Ar atmosphere at a rate of 10 °C min^{-1} is shown in Fig. 5. The weight change of the sample after the heating–cooling run amounted to less than 0.5%. Small endothermal peaks are observed upon heating, at *ca.* 1340 and 1380 °C, before $Mn_3Ta_2O_8$ melts at *ca.* 1470 °C. These may either

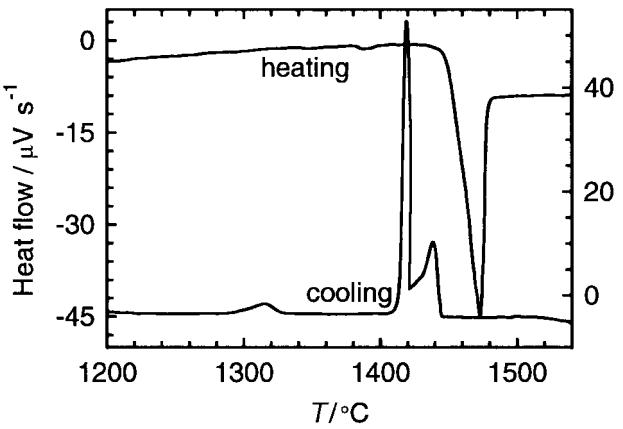

Fig. 5 DTA recordings for $Mn_3Ta_2O_8$ heated and then cooled in Ar atmosphere.

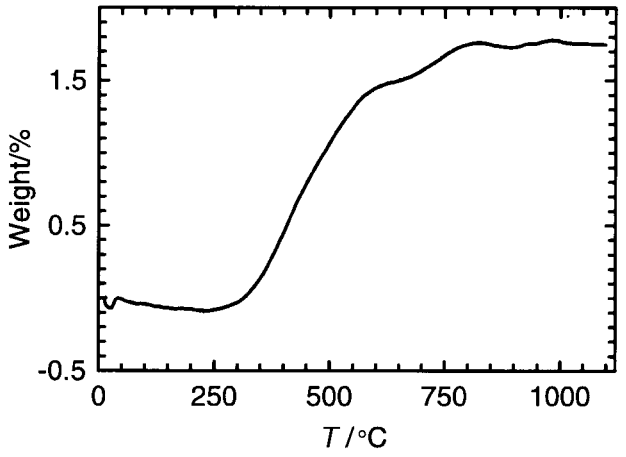

Fig. 6 TG curve for the oxidation of $Mn_3Ta_2O_8$ in air.

originate from phase transitions of $Mn_3Ta_2O_8$ or be associated with the impurity phases $MnTa_2O_6$ and $Mn_4Ta_2O_9$ present. Upon cooling, an exothermal reaction starts at approximately 1440 °C, characteristic of a passage through a liquidus curve and subsequent eutectic or peritectic solidification. In addition, a smaller exothermal transition occurs at *ca.* 1320 °C, indicating a solid-state phase transition.

A TG recording of the oxidation of $Mn_3Ta_2O_8$ in air upon heating, at a rate of 5 °C min^{-1}, is shown in Fig. 6. The largest part of the oxidation occurs in the temperature range 300–600 °C and is exothermal. A following smaller increase in weight is observed up to *ca.* 850 °C, and two broad endothermal reactions take place above 600 °C. The calculated metal–oxygen compositions at the observed plateaus at 600 and 850 °C are $MO_{1.72}$ and $MO_{1.75}$, respectively.

A Guinier–Hägg film of the sample heated to 1100 °C in the TG run showed that a new phase had formed. Its powder pattern could be indexed by a monoclinic unit cell with $a=4.7574(5)$, $b=5.7296(6)$, $c=5.1133(3)$ Å, $\beta=91.202(9)°$ and $V=139.35$ Å^3. The pattern also contained reflections from tetragonal Mn_3O_4 (JCPDS No. 24-734) and three additional reflections, with relative intensities below 6%, which could not be attributed to any reported oxide containing Mn and/or Ta. The indexed pattern for the new phase is given in Table 4 for the first 20 observed lines. The unit cell, systematic reflection absences ($h0l$, $l \neq 2n$), and the reflection intensities strongly suggest that the phase is of the wolframite ($FeWO_4$) type.[13] Its structure, composition and formation will be further investigated.

Table 4 Observed and calculated 2θ values for the Guinier–Hägg diffraction pattern of the Mn–Ta wolframite type phase up to the twentieth observed line. $\Delta 2\theta = 2\theta_{obs} - 2\theta_{calc}$ [$\lambda = 1.5406$ Å, cell figure-of-merit: $M_{20}=85$, $F_{20}=92$ (0.0063, 35)].

hkl	$2\theta_{obs}$/degrees	$\Delta 2\theta$/degrees	d_{obs}/Å	I/I_0
0 1 0	15.464	0.011	5.73	1
1 0 0	18.640	0.000	4.756	9
0 1 1	23.305	0.004	3.814	8
1 1 0	24.295	−0.006	3.661	50
−1 1 1	29.770	0.001	2.999	99
1 1 1	30.230	−0.008	2.954	100
0 2 0	31.183	−0.013	2.866	19
0 0 2	35.082	0.003	2.556	30
0 2 1	35.904	−0.001	2.4992	55
2 0 0	37.796	−0.002	2.3783	17
−1 0 2	39.656	0.010	2.2709	4
1 2 1	40.934	0.002	2.2029	8
−1 1 2	42.797	0.007	2.1113	9
1 1 2	43.494	0.018	2.0790	10
2 1 1	45.196	−0.013	2.0046	3
0 2 2	47.638	−0.004	1.9074	10
2 2 0	49.792	0.001	1.8298	11
1 3 0	51.533	0.010	1.7720	35
−2 0 2	51.928	0.006	1.7595	18
−2 2 1	52.828	0.004	1.7316	23

Concluding remarks

There are a large number of structures related to the fluorite structure, which can be derived from it by ordered removal of oxygen atoms or ordering of metal atoms. $Mn_3Ta_2O_8$ is a new member of this class of compounds. Among the cations of the first-row transition metals the largest ionic radius is found for Mn^{2+}, and the crystal chemistry of oxides containing Mn^{2+} and Ta^{5+} ions is expected to be influenced by this fact and by the comparatively large difference in size of these cations. The stability of fluorite-related structures increases with the size of the cation, and such structures may therefore be expected for higher Mn^{2+} contents. The metal-to-oxygen ratio decreases with increasing Mn^{2+} content, however, and the Mn-rich compounds $Mn_4Ta_2O_9$ ($MO_{1.5}$) and $Mn_{11}Ta_4O_{21}$ ($MO_{1.4}$)[4] have structures that are related to corundum. The $Mn_3Ta_2O_8$ compound is accordingly found at an Mn–Ta–O composition that satisfies both a relatively high metal-to-oxygen ratio, $MO_{1.6}$, and a high Mn content.

We have not been able to determine the superstructure, implied by the ED studies of $Mn_3Ta_2O_8$, from the present X-ray synchrotron data. It is very likely, however, that the superstructure, with $c'=6c$, is associated with either modulations of oxygen atom positions and/or an extended ordering of oxygen atoms around Mn2 and Mn3.

Finally, it can be remarked that presently available data indicate a series of uncharacterised phases in the system Mn^{2+}–Mn^{3+}–Ta^{5+}–O, among them the wolframite type phase mentioned above and the phases denoted by Turnock[1] as $MnTaO_4$ and $Mn_{1.4}TaO_{4.2}$. Studies of phase formation and crystal structures in these systems are presently in progress. We have recently characterised a new cubic fluorite phase $Mn_{0.6}Ta_{0.4}O_{1.65}$ by techniques which include XRPD, selected-area ED and high-resolution electron microscopy.[14] The ED patterns of the phase exhibit prominent diffuse scattering, similar to that reported for other cubic oxygen-deficient fluorite compounds.

The authors thank Dr. T. Hörlin for help with the conductivity measurements. Prof. M. Nygren is thanked for help with the thermal analysis and for support and valuable discussions. This work has been financially supported by the Swedish Natural Science Foundation.

References

1 A. C. Turnock, *J. Am. Ceram. Soc.*, 1966, **49**, 382.
2 N. Schönberg, *Acta Metall.*, 1955, **3**, 14.
3 J. Grins, P.-O. Käll and G. Svensson, *J. Solid State Chem.*, 1995, **117**, 48.
4 J. Grins and A. Tyutyunnik, *J. Solid State Chem.*, 1998, **137**, 276.
5 M. A. Subramanian, G. Aravamudan and G. V. Subba Rao, *Prog. Solid State Chem.*, 1983, **1**, 55.
6 R. Norrestam, *Ark. Kemi*, 1968, **29**, 343.
7 G. Cascarano, L. Favia and C. Giacovazzo, *J. Appl. Crystallogr.*, 1992, **25**, 310.
8 A. C. Larson and R. B. Von Dreele, Los Alamos National Laboratory Report No. LA-UR-86-748, 1987.
9 T. Hörlin, *Chem. Scr.*, 1985, **25**, 270.
10 P.-E. Werner, L. Eriksson and M. Westdahl, *J. Appl. Crystallogr.*, 1985, **18**, 367.
11 I. D. Brown and D. Altermatt, *Acta Crystallogr., Sect. B*, 1985, **41**, 244.
12 R. D. Shannon, *Acta Crystallogr., Sect A*, 1965, **32**, 258.
13 H. Weitzel, *Z. Kristallogr.*, 1976, **144**, 238.
14 S. Esmaeilzadeh, J. Grins and A.-K. Larsson, in preparation.

Paper 8/04938K